



PERGAMON

International Journal of Solids and Structures 39 (2002) 2087–2108

INTERNATIONAL JOURNAL OF
**SOLIDS and
STRUCTURES**

www.elsevier.com/locate/ijsolstr

A material derivative approach in design sensitivity analysis of three-dimensional contact problems

Nam Ho Kim¹, Kiyong Yi, Kyung Kook Choi^{*}

*The Center for Computer-Aided Design, Department of Mechanical Engineering, College of Engineering,
208 Engineering Research Facility, The University of Iowa, Iowa City, IA 52242-1000, USA*

Received 2 August 2001; received in revised form 29 December 2001

Abstract

A shape design sensitivity analysis (DSA) and the optimization of a three-dimensional (3-D) contact problem is proposed using a material derivative approach. A penalty-regularized contact variational equation is differentiated with respect to the shape design parameter. A die shape DSA is also carried out by defining a design velocity field at rigid-body geometry. The material derivative that is consistent with the frictional return-mapping scheme is derived by using nonassociative plasticity. A linearized design sensitivity equation is solved without iteration by using a meshfree method at each converged load step. In order to improve the convergence behavior of the contact problem, a C^2 -continuous contact surface is constructed from the scattered set of particles. The accuracy and efficiency of the proposed method is shown using two-dimensional and 3-D design examples of the DSA and optimization process. © 2002 Elsevier Science Ltd. All rights reserved.

Keywords: Design sensitivity analysis; Design optimization; Contact problem; Smooth contact surface; Meshfree method

1. Introduction

Although many engineering applications include contact constraints, slow progress has been made in design sensitivity analysis (DSA) and optimization, especially as compared to the fast growth in structural DSA of noncontact problem. This is partly due to the complicated kinematics involved in contact analysis, and the theoretical depth required in variational inequality. The effect of contact constraint on structural performance must be taken into account in designing structural components that make contact with other parts. In the sheet metal stamping process, for example, a die shape design is critical to control workpiece shape after spring-back, to reduce wrinkling effects, and to remove the phenomena of necking. A die shape design parameter exerts its influence on structural performance through the contact constraint. In this

^{*} Corresponding author. Tel.: +1-319-335-3380/5684; fax: +1-319-335-5669/3380.

E-mail address: kkchoi@ccad.uiowa.edu (K.K. Choi).

¹ Current Address: Department of Mechanical Engineering, The University of Florida, Gainesville, FL 32611, USA.

paper, three-dimensional (3-D) contact DSA and optimization are developed by extending previous two-dimensional (2-D) research results (Kim et al., 2000).

The DSA of a contact problem has been approached from the mathematical perspective, in which the variational inequality is differentiated to obtain design sensitivity variational inequality. By understanding the variational inequality as a projection, Mignot (1976) proved that the projection onto the convex cone (constraint set) is directionally differentiable. Sokolowski and Zolesio (1991) derived a shape sensitivity formulation for the variational inequality from Mignot's result. They conclude that the solution to the variational inequality is directionally differentiable, and its shape sensitivity is a solution to another variational inequality, which is a projection onto a common convex set of tangential and orthogonal subspaces.

Because there is no mathematical proof for the existence of design sensitivity for nonlinear problems, the approximated variational equation or finite element matrix equation has been differentiated to accommodate many engineering applications. Spivey and Tortorelli (1994) presented a sensitivity formulation of the nonlinear frictionless contact problem for a beam, and optimized the geometry of the rigid surface. Antunez and Kleiber (1996) derived a sensitivity formulation of the contact problem using a flow approach to analyze the structure. Pollock and Noor (1996) developed a nonlinear dynamic sensitivity formulation using the discrete DSA method by differentiating the finite element matrix equation. Maniatty and Chen (1996) developed a design sensitivity formulation for the steady state metal-forming process using a semi-analytical adjoint variable method. Zhao et al. (1997) solved an unconstrained optimization problem to minimize the difference between the shape of the stamped workpiece and the desired shape. Their sensitivity equation requires an additional tangent stiffness matrix that is different from the one used in response analysis. Chung and Hwang (1998) proposed a method for transient forming process optimization. Since a semi-analytical method is used to compute the sensitivity coefficient, accuracy depends on the size of the design perturbation. Recently, Zabarar et al. (2000) applied die shape DSA to the 2-D metal-forming process. However, a general 3-D contact DSA method that includes a large deformation in the elastoplastic material and complicated frictional behavior is not reported in the literature. In this paper, shape DSA of a 3-D contact problem is developed using the material derivative approach. Instead of the variational inequality, a penalty-regularized variational equation is differentiated with respect to the structural shape and die shape design parameters. The material derivative that is consistent with the frictional return-mapping scheme is derived.

Discretization of the nonlinear equation and the design sensitivity equation is carried out using the meshfree method (Liu et al., 1995; Chen et al., 1996), where the structural domain is represented by a set of particles. The meshfree shape function is obtained from a set of supporting particles around an integration point to satisfy a reproducing condition, which exactly represents a certain order of polynomials. In contrast to finite element analysis, the construction of a shape function is independent of the mesh geometry in the meshfree method. Thus, this method is attractive for both a large deformation problem and a large shape-changing design problem, in which initially regular mesh can be significantly distorted during nonlinear analysis and during the shape optimization process. However, since the proposed approach is based on the continuum method, other discretization methods are easily applicable using the minimum implementation effort.

A piecewise-linear contact surface causes a significant amount of difficulty in the Newton-type iterative method because it lacks continuity across the surface boundary. From a computational point of view, a C^2 -continuous surface is required to guarantee a continuous contact force across the boundary. A piecewise C^3 -continuity is additionally required to provide a valid tangent stiffness matrix at each surface. In the finite element-based method, however, it is difficult to generate such regular surface patches. In this paper, a meshfree technique is used to produce a smooth surface from a set of scattered particles whose connectivity information is not provided in advance (Wang, 2000).

The frictional mechanism is modeled using a nonassociative plasticity (Michalowski and Mroz, 1978). Since the friction force and the contact location at the previous load step are required to calculate friction

force at the current load step, the design sensitivity equation is path dependent. The computational cost of DSA, however, is still very low compared to nonlinear contact analysis where an iterative solution process is required. Moreover, DSA uses the same tangent stiffness matrix as response analysis, which is already decomposed during contact analysis; all that is required is a substitution process using different right-hand side vectors. The computational cost of DSA is about 5–10% that of response analysis, which is shown using the numerical example of a rubber gasket and metal extrusion problem.

The composition of this paper is as follows. In Section 2, a brief review of nonlinear contact analysis is presented. Since the purpose is to develop DSA, contact analysis explanations are kept to a minimum. A design sensitivity formulation is presented in Section 3 using material derivative approach. The contact sensitivity formulation is further extended in Section 4 when friction exists between contact surfaces. A smooth contact surface is generated using a meshfree interpolation method in Section 5 to improve convergence behavior of the contact problem. Numerical examples and design optimization results are shown in Section 6. Accuracy of the proposed sensitivity computation is compared to that using the finite difference method.

2. Review of the contact analysis

In this section, contact analysis is described in the continuum formulation for a large deformation problem. The contact problem is defined as a variational inequality, which is equivalent to the minimization problem with constraints in contact kinematics. For further information on the numerical treatment of contact constraints, the mathematical programming method (Klarbring, 1986; Kwak, 1991), active set strategies (Luenberger, 1984), and the sequential quadratic programming method (Barthold and Bischoff, 1988) are available. The active set strategy can be applied in combination with the Lagrange multiplier method or the penalty method. In this paper, the penalty regularization method is used to approximate the contact variational inequality.

2.1. Contact kinematics

A brief review of contact analysis is presented to introduce notations that appear in the following DSA section. Throughout this paper, X represents the undeformed configuration, while x represents the current configuration. Fig. 1 shows the contact situation between two bodies, represented by Ω_x^1 and Ω_x^2 . Ω_x^1 is called a slave body, while Ω_x^2 is a master body, although such a distinction is inconsequential in continuum formulation. Likewise, a part of the boundary Γ_x^1 in Ω_x^1 is called a slave surface, and a part of the boundary Γ_x^2 in Ω_x^2 is called a master surface. The counterparts of Γ_x^1 and Γ_x^2 at the undeformed configuration will be denoted as Γ_X^1 and Γ_X^2 , respectively. Contact constraints are imposed such that the points on Γ_x^1 cannot penetrate into Γ_x^2 . Let the master surface Γ_x^2 be represented by the two parameters ξ_1 and ξ_2 such that a surface point $x^c \in \Gamma_x^2$ can be expressed as $x^c(\xi_1, \xi_2)$.

As will be explained in Section 5, it is assumed that the master surface is smooth enough for all required derivatives to be computed in the parametric domain. Two tangential vectors in the parametric direction on the master surface are defined as

$$e_\alpha = x_{,\alpha}^c, \quad \alpha = 1, 2 \quad (1)$$

where the subscripted comma denotes a partial derivative with respect to the parametric coordinate, i.e., $x_{,\alpha} = \partial x / \partial \xi_\alpha$, $\alpha = 1, 2$. In this paper, Greek letters are used for the index in the direction of the parametric coordinates. In the case of a 2-D contact problem, $\alpha = 1$. Note that e_1 and e_2 are not necessarily orthogonal to each other, but are tangent to the contact surface. The unit outward normal vector on the master surface can be obtained using Eq. (1) as

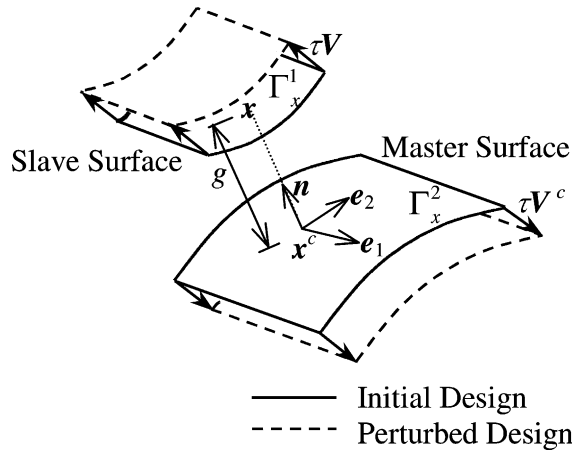


Fig. 1. Contact kinematics and design velocities of two bodies.

$$\mathbf{n} = \frac{\mathbf{e}_1 \times \mathbf{e}_2}{\|\mathbf{e}_1 \times \mathbf{e}_2\|} \tag{2}$$

One of the most important steps in contact analysis process is locating the contact point in an accurate and efficient way. The contact point $\mathbf{x}^c \in \Gamma_x^2$ corresponding to the slave point $\mathbf{x} \in \Gamma_x^1$ can be found from the following consistency condition:

$$\mathbf{e}_\alpha \cdot (\mathbf{x} - \mathbf{x}^c) = 0, \quad \alpha = 1, 2 \tag{3}$$

which provides the closest projection point \mathbf{x}^c of \mathbf{x} , and the corresponding parametric coordinates at the contact point are denoted by (ξ_1^c, ξ_2^c) . For general surface Γ_x^2 , no explicit form of the solution to Eq. (3) is available. Finding contact point \mathbf{x}^c efficiently is very important for a large deformation problem. A local Newton method can be used to solve nonlinear equation (3) with a close initial estimate.

The gap function is defined by the distance between two contact points as

$$g = \mathbf{n} \cdot (\mathbf{x} - \mathbf{x}^c) \geq 0 \tag{4}$$

where the inequality constraint represents the impenetrability condition: the slave point cannot penetrate the slave surface. The violated region of constraint Eq. (4) will be penalized as shown in the following section.

2.2. Variational formulation and penalty method

The weak formulation of the contact variational inequality (see Kikuchi and Oden (1988)) is to find displacement field $\mathbf{z} \in V$, such that

$$a_\Omega(\mathbf{z}, \mathbf{w} - \mathbf{z}) \geq \ell_\Omega(\mathbf{w} - \mathbf{z}) \quad \forall \mathbf{w} \in V \tag{5}$$

where $a_\Omega(\mathbf{z}, \mathbf{w})$ is the structural energy form, and $\ell_\Omega(\mathbf{w})$ is the load linear form. In Eq. (5), V is the constraint set that satisfies the impenetrability condition in Eq. (4). It is shown by Kikuchi and Oden (1988) that the inequality in Eq. (5) is equivalent to the constrained minimization problem, which can be approximated using the Lagrange multiplier or penalty method. In this paper, the penalty method is chosen to approximate Eq. (5), without introducing additional unknowns into the variational equation.

If a region called $\Gamma_x^c (\subset \Gamma_x^1)$ exists that violates the impenetrability condition of Eq. (4), then this region is penalized using a penalty function defined as

$$P(\mathbf{x}, \mathbf{x}^c) = \frac{1}{2} \omega_N \int_{\Gamma_x^c} g^2 d\Gamma \tag{6}$$

where ω_N is the penalty parameter. Let the symbol “over-bar” denote a variation of the quantity such that $\bar{\mathbf{z}}$ represents the displacement variation. The variation of the penalty function in Eq. (6) contains the variation of the gap function, which can be obtained from its definition as

$$\bar{g} = \mathbf{n} \cdot (\bar{\mathbf{z}} - \bar{\mathbf{z}}^c) \equiv \mathbf{n} \cdot \hat{\bar{\mathbf{z}}} \tag{7}$$

where the notations $\hat{\mathbf{z}} = \mathbf{z} - \mathbf{z}^c$ and $\hat{\bar{\mathbf{z}}} = \bar{\mathbf{z}} - \bar{\mathbf{z}}^c$ are used for the relative displacement between two contact points. Note that the variation of the normal vector vanishes because of the orthogonal condition with vector $(\mathbf{z} - \mathbf{z}^c)$. The variation of the penalty function in Eq. (6) leads to the contact form, defined as

$$\bar{P} \equiv b_N(\mathbf{z}, \bar{\mathbf{z}}) = \omega_N \int_{\Gamma_{xc}} \mathbf{g}\mathbf{n} \cdot \hat{\bar{\mathbf{z}}} d\Gamma \tag{8}$$

From a virtual work point of view, the contact form in Eq. (8) can be understood as the work done by contact force $\omega_N \mathbf{g}\mathbf{n}$ during the virtual displacement $\bar{\mathbf{z}} - \bar{\mathbf{z}}^c$.

By combining Eq. (8) with Eq. (5), the approximated variational equation for penalized contact condition becomes

$$a_\Omega(\mathbf{z}, \bar{\mathbf{z}}) + b_N(\mathbf{z}, \bar{\mathbf{z}}) = \ell_\Omega(\bar{\mathbf{z}}) \quad \forall \bar{\mathbf{z}} \in Z \tag{9}$$

Note that, even if a linear constitutive model is used, Eq. (9) is nonlinear because the inequality constraint is imposed through the penalty method on the deformation field. In Eq. (9),

$$Z = \left\{ \mathbf{z} \in [H^1(\Omega)]^3 \mid \mathbf{z}(\mathbf{x}) = \mathbf{0}, \quad \mathbf{x} \in \Gamma_g \right\} \tag{10}$$

is the space of kinematically admissible displacements, $H^1(\Omega)$ is first-order Sobolev space, and Γ_g is the essential boundary where the displacement is prescribed.

Since the purpose of this paper is to develop a contact DSA method, references will be provided for more detailed discussions of structural aspects. In this paper, an elastoplastic material with a combined isotropic and kinematic hardening model is used. In order to handle a finite deformation problem, it is assumed that the deformation gradient is constructed by multiplying elastic and plastic parts (Simo, 1992). Fig. 2 summarizes the structural energy and applied load forms. Since Kirchhoff stress σ_{ij} is used for the stress measure, the integration domain of the structural energy form is the undeformed configuration. For simplicity, only a conservative load is considered in which the applied load is independent of the displacement.

Structural Energy Form: $a_\Omega(\mathbf{z}, \bar{\mathbf{z}}) = \int_{\Omega_x} \sigma_{ij} \varepsilon_{ij}(\bar{\mathbf{z}}) d\Omega$

Applied Load Form: $\ell_\Omega(\bar{\mathbf{z}}) = \int_{\Omega_x} \bar{z}_i f_i^b d\Omega + \int_{\Gamma_x^s} \bar{z}_i f_i^s d\Gamma$

Linearized Structural Energy Form:

$$a_\Omega^*(\mathbf{z}; \Delta \mathbf{z}, \bar{\mathbf{z}}) = \int_{\Omega_x} [\varepsilon_{ij}(\bar{\mathbf{z}}) c_{ijkl} \varepsilon_{kl}(\Delta \mathbf{z}) + \sigma_{ij} \eta_{ij}(\Delta \mathbf{z}, \bar{\mathbf{z}})] d\Omega$$

Fig. 2. Structural analysis with elastoplastic constitutive model.

2.3. Linearization

The nonlinear variational equation (9) can be solved using a Newton iterative method through linearization. The exact tangent operator plays an important role in the convergence rate. Linearization of the structural energy form depends on the constitutive model, which can be found in the literature (Hughes, 1987; Simo, 1992). Let the linearization of a function $f(\mathbf{x})$ in the direction of $\Delta \mathbf{z}$ be denoted as

$$L[f] \equiv \left. \frac{d}{d\varepsilon} f(\mathbf{x} + \varepsilon \Delta \mathbf{z}) \right|_{\varepsilon=0} = \frac{\partial f}{\partial \mathbf{x}} \Delta \mathbf{z} \quad (11)$$

then, the linearization of $a_\Omega(\mathbf{z}, \bar{\mathbf{z}})$ and $b_N(\mathbf{z}, \bar{\mathbf{z}})$ becomes

$$L[a_\Omega(\mathbf{z}, \bar{\mathbf{z}})] = a_\Omega^*(\mathbf{z}; \Delta \mathbf{z}, \bar{\mathbf{z}}) \quad (12)$$

$$L[b_N(\mathbf{z}, \bar{\mathbf{z}})] = b_N^*(\mathbf{z}; \Delta \mathbf{z}, \bar{\mathbf{z}}) \quad (13)$$

where $\Delta \mathbf{z}$ is the displacement increment and $a_\Omega^*(\mathbf{z}; \bullet, \bullet)$ is symmetric in its arguments. In case of an elastoplastic material, the expression of $a_\Omega^*(\mathbf{z}; \Delta \mathbf{z}, \bar{\mathbf{z}})$ is given in Fig. 2. The expression of $b_N^*(\mathbf{z}; \Delta \mathbf{z}, \bar{\mathbf{z}})$ can be found in Laursen and Simo (1993), which will be derived in the next section for DSA.

The linearization of the contact variational form in Eq. (13) is combined with that of the structural energy form in Eq. (12) to set up an incremental system of equations. Let the left superscript n denote the current configuration time t_n , and let the right superscript k denote the current iteration counter. The linearized incremental equation is

$$a_\Omega^*({}^n \mathbf{z}^k; \Delta \mathbf{z}^{k+1}, \bar{\mathbf{z}}) + b_N^*({}^n \mathbf{z}^k; \Delta \mathbf{z}^{k+1}, \bar{\mathbf{z}}) = \ell_\Omega(\bar{\mathbf{z}}) - a_\Omega({}^n \mathbf{z}^k, \bar{\mathbf{z}}) - b_N({}^n \mathbf{z}^k, \bar{\mathbf{z}}) \quad \forall \bar{\mathbf{z}} \in Z \quad (14)$$

For a given load step, Eq. (14) is solved iteratively until the right side, residual force, vanishes. After convergence, the decomposed tangent stiffness operator is stored to be used during DSA.

3. Design sensitivity analysis of a contact problem

In this section, a shape sensitivity formulation is developed for the contact variational equation using the material derivative approach. Even if a structure deforms during the nonlinear response analysis, the material derivative is always taken at the undeformed configuration. This is the reason to use the total Lagrangian formulation over the updated Lagrangian formulation in which the current configuration is considered as a reference frame. The basic formulas for material derivatives in nonlinear analysis can be found in Choi (1993). In the contact problem, the transformation to the undeformed configuration is simple, using the relation $\mathbf{x} = \mathbf{X} + \mathbf{z}$ where \mathbf{x} and \mathbf{X} are spatial and material coordinates, respectively.

3.1. Material derivative formulas

In shape DSA, a material point \mathbf{X} is moved to a new point $\mathbf{X}_\tau (= \mathbf{X} + \tau \mathbf{V})$ because of design perturbation. A design velocity field $\mathbf{V}(\mathbf{X})$ represents the direction of the design perturbation, and τ is a scalar parameter to control the perturbation size (see Fig. 1). Since the contact constraint is related to the current coordinate of a material point, the following derivatives are required. The material derivative of the structural point $\mathbf{x} \in \Omega_x$ at the current configuration becomes

$$\left. \frac{d}{d\tau} (\mathbf{x}_\tau) \right|_{\tau=0} \equiv \left. \frac{d}{d\tau} (\mathbf{X}_\tau + \mathbf{z}_\tau) \right|_{\tau=0} = \mathbf{V}(\mathbf{X}) + \dot{\mathbf{z}}(\mathbf{X}) \quad (15)$$

The superposed dot (for example, $\dot{\mathbf{z}}$) will be used to denote the material derivative of a function throughout this paper. On the other hand, the perturbation of the contact point \mathbf{x}^c on the master surface Γ_x^c can be obtained by using the chain rule and by perturbing the natural coordinate corresponding to the contact point in the tangential direction as

$$\left. \frac{d}{d\tau} (\mathbf{x}_\tau^c) \right|_{\tau=0} = \mathbf{V}^c + \dot{\mathbf{z}}^c + \mathbf{e}_\alpha \dot{\xi}_\alpha \quad (16)$$

where a summation rule is used for the repeated indices. The contact point is perturbed by satisfying the contact consistency condition, in addition to satisfying its own design velocity fields and displacement sensitivity.

The material derivatives of the structural energy and applied load forms depend on the constitutive model used. For a general nonlinear material model that includes elastoplasticity, the material derivative of the structural energy form can be expressed (Kim et al., 2001) as

$$\left. \frac{d}{d\tau} [a_\Omega(\mathbf{z}_\tau, \bar{\mathbf{z}}_\tau)] \right|_{\tau=0} = a_\Omega^*(\mathbf{z}; \dot{\mathbf{z}}, \bar{\mathbf{z}}) + a'_V(\mathbf{z}, \bar{\mathbf{z}}) \quad (17)$$

where $a_\Omega^*(\mathbf{z}; \dot{\mathbf{z}}, \bar{\mathbf{z}})$ is the same form as the linearized structural energy form defined in Eq. (12) by substituting $\Delta \mathbf{z}$ into $\dot{\mathbf{z}}$. As its expression is given in Fig. 3, $a'_V(\mathbf{z}, \bar{\mathbf{z}})$ is called the structural fictitious load form, which is linear in V and contains all known terms from response analysis and DSA up to the previous load step. The material derivative of the applied load form is independent of the displacement, when conservative load is considered, as

$$\left. \frac{d}{d\tau} [\ell_\Omega(\bar{\mathbf{z}}_\tau)] \right|_{\tau=0} = \ell'_V(\bar{\mathbf{z}}) \quad (18)$$

<p>Explicit Term</p> $\varepsilon_{ij}^v(\mathbf{z}) = -sym\left(\frac{\partial z_i}{\partial X_k} \frac{\partial V_k}{\partial x_j}\right),$ $\eta_{ij}^v(\mathbf{z}, \bar{\mathbf{z}}) = -sym\left(\frac{\partial \bar{z}_k}{\partial x_i} \frac{\partial z_k}{\partial X_m} \frac{\partial V_m}{\partial x_j} + \frac{\partial \bar{z}_i}{\partial X_k} \frac{\partial V_k}{\partial x_j}\right)$ <p>Path-dependent Term</p> $\varepsilon_{ij}^p(\mathbf{z}) = -sym(G_{ij})$ $\eta_{ij}^p(\mathbf{z}, \bar{\mathbf{z}}) = -sym\left(\frac{\partial \bar{z}_i}{\partial x_k} G_{kj} + \frac{\partial \bar{z}_k}{\partial x_i} G_{kj}\right)$ $\mathbf{G} = \mathbf{F}^e \dot{\mathbf{F}}^p \mathbf{F}^{-1}$ <p>Structural Fictitious Load Form</p> $a'_V(\mathbf{z}, \bar{\mathbf{z}}) = \int_{\Omega_x} [\varepsilon_{ij}(\bar{\mathbf{z}}) c_{ijkl} \varepsilon_{kl}^v(\mathbf{z}) + \sigma_{ij} \eta_{ij}^v(\mathbf{z}, \bar{\mathbf{z}}) + \sigma_{ij} \varepsilon_{ij}(\bar{\mathbf{z}}) div V] d\Omega$ $+ \int_{\Omega_x} [\varepsilon_{ij}(\bar{\mathbf{z}}) c_{ijkl} \varepsilon_{kl}^p(\mathbf{z}) + \sigma_{ij} \eta_{ij}^p(\mathbf{z}, \bar{\mathbf{z}}) + \sigma_{ij}^{fc} \varepsilon_{ij}(\bar{\mathbf{z}})] d\Omega$ <p>External Fictitious Load</p> $\ell'_V(\bar{\mathbf{z}}) = \int_{\Omega_x} [\bar{\mathbf{z}} \cdot (\nabla_x \mathbf{f}^b \cdot \mathbf{V}) + \bar{\mathbf{z}} \cdot \mathbf{f}^b div V] d\Omega$ $+ \int_{\Gamma_x} [\bar{\mathbf{z}} \cdot (\nabla_x \mathbf{f}^s \cdot \mathbf{V}) + \kappa \bar{\mathbf{z}} \cdot \mathbf{f}^s V_n] d\Gamma$

Fig. 3. Structural DSA formulas (Kim et al., 2001).

Note that the structural fictitious load form $a'_V(\mathbf{z}, \bar{\mathbf{z}})$ is path independent for elastic material such that $a'_V(\mathbf{z}, \bar{\mathbf{z}})$ requires the results of response analysis at the current load step, and design velocity information at the undeformed configuration. However, for elastoplastic material, $a'_V(\mathbf{z}, \bar{\mathbf{z}})$ also requires the sensitivity results of the plastic variables at the previous load step, which makes DSA path dependent.

3.2. Design sensitivity analysis of a contact problem

Instead of differentiating the variational inequality for contact DSA, the penalty-approximated variational equation is differentiated with respect to the shape design parameter. In case of the flexible-rigid contact problem, the shape change of the master surface is equivalent to the die shape design problem. Thus, a unified design sensitivity formulation can be derived for structural shape and die shape design problems.

To begin, let the contact surface Γ_X^c change its shape due to design perturbation. The contact form of Eq. (8) depends on the design in two ways: explicitly through the contact surface change and implicitly through the response \mathbf{z} . The material derivative of the contact form can be obtained as

$$\frac{d}{d\tau} [b_N(\mathbf{z}_\tau, \bar{\mathbf{z}}_\tau)] \Big|_{\tau=0} = \omega_n \int_{\Gamma_X^c} [\dot{\bar{\mathbf{g}}}\bar{\mathbf{g}} + g\dot{\bar{\mathbf{g}}} + g\bar{\mathbf{g}}\kappa V_n] d\Gamma \tag{19}$$

where κ is the curvature of the master surface, and V_n is the normal component of the design velocity. The purpose of the following derivations is to express $\dot{\bar{\mathbf{g}}}$ and $\dot{\bar{\mathbf{z}}}$ in terms of $\dot{\mathbf{z}}$ and \mathbf{V} , and the implicit term $\dot{\mathbf{z}}$ is then obtained in terms of the explicit term \mathbf{V} .

From its definition in Eq. (4), the material derivative of the gap function can be obtained as

$$\dot{\bar{\mathbf{g}}} = \mathbf{n} \cdot (\dot{\mathbf{z}} + \hat{\mathbf{V}}) \tag{20}$$

where $\hat{\mathbf{V}} = \mathbf{V} - \mathbf{V}^c$. Note that $\dot{\bar{\mathbf{g}}}$ only has a normal component of the variation. The material derivative of $\bar{\mathbf{g}}$, however, is not straightforward. The outline of the derivation is provided as follows. From its definition in Eq. (7), it is necessary to differentiate the unit normal vector in Eq. (2) as

$$\frac{d}{d\tau} \mathbf{n}_\tau \Big|_{\tau=0} = -(\mathbf{n} \cdot \dot{\mathbf{e}}_\alpha) \mathbf{e}^\alpha \tag{21}$$

where \mathbf{e}^α is the dual basis of \mathbf{e}_α and has the following relation:

$$\begin{aligned} \mathbf{e}^\alpha \cdot \mathbf{e}_\beta &= \delta_{\alpha\beta} \\ \mathbf{e}^\alpha &= m_{\alpha\beta}^{-1} \mathbf{e}_\beta \end{aligned} \tag{22}$$

with $m_{\alpha\beta} = \mathbf{e}_\alpha \cdot \mathbf{e}_\beta$. In Eq. (21),

$$\dot{\mathbf{e}}_\alpha \equiv \frac{d}{d\tau} (\mathbf{x}_{,\alpha}^c) \Big|_{\tau=0} = \dot{\mathbf{z}}_{,\alpha}^c + \mathbf{V}_{,\alpha}^c + \mathbf{x}_{,\alpha\beta}^c \dot{\xi}_\beta \tag{23}$$

By using Eqs. (21) and (23), the material derivative of $\bar{\mathbf{g}}$ can be expressed as

$$\dot{\bar{\mathbf{g}}} = \frac{d}{d\tau} [(\bar{\mathbf{z}} - \bar{\mathbf{z}}^c) \cdot \mathbf{n}] \Big|_{\tau=0} = -\mathbf{n} \cdot \bar{\mathbf{z}}_{,\alpha}^c \dot{\xi}_\alpha - \mathbf{n} \cdot \dot{\mathbf{e}}_\alpha \bar{\xi}_\alpha + g(\mathbf{n} \cdot \dot{\mathbf{e}}_\beta) m_{\alpha\beta}^{-1} (\mathbf{n} \cdot \bar{\mathbf{e}}_\alpha) \tag{24}$$

Thus, it is only necessary to calculate the expression of $\dot{\xi}_\alpha$ in terms of $\dot{\mathbf{z}}$ and \mathbf{V} . The expression of $\dot{\xi}_\alpha$ can be obtained by differentiating the consistency condition in Eq. (3) as

$$\frac{d}{d\tau} [(\mathbf{x} - \mathbf{x}^c) \cdot \mathbf{e}_\alpha] \Big|_{\tau=0} = 0, \quad \alpha = 1, 2 \tag{25}$$

After rearrangement, $\dot{\xi}_x$ is expressed in terms of \dot{z} and V as

$$\dot{\xi}_x = A_{\alpha\beta}^{-1}[\hat{z} \cdot e_\beta + gn \cdot \dot{z}_{,\beta}^c] + A_{\alpha\beta}^{-1}[\hat{V} \cdot e_\beta + gn \cdot V_{,\beta}^c] \equiv \zeta_x(\dot{z}) + \zeta_x(V) \quad (26)$$

with

$$A_{\alpha\beta} = m_{\alpha\beta} - gn \cdot x_{,\alpha\beta}^c \quad (27)$$

Note that $A_{\alpha\beta}$ is also the coefficient matrix that appears in the Newton iteration to find the closest contact point in Eq. (3).

By substituting Eq. (26) into Eq. (24), and by using the expression of Eq. (20), the material derivative of the contact form can be expressed in terms of \dot{z} and V . Since the objective of DSA is to solve the implicitly dependent parts in terms of the explicitly dependent parts, the material derivative of the contact form in Eq. (19) is separated into two parts as

$$\frac{d}{d\tau} [b_N(z_\tau, \bar{z}_\tau)] \Big|_{\tau=0} \equiv b_N^*(z; \dot{z}, \bar{z}) + b'_N(z, \bar{z}) \quad (28)$$

where

$$\begin{aligned} b_N^*(z; \dot{z}, \bar{z}) = & \omega_N \int_{\Gamma_X^c} \hat{z} \cdot nn \cdot \hat{z} d\Gamma - \omega_N \int_{\Gamma_X^c} g[n \cdot \bar{z}_{,\alpha}^c \zeta_x(\dot{z}) + n \cdot \dot{z}_{,\alpha}^c \bar{\zeta}_x + n \cdot x_{,\alpha\beta}^c \bar{\zeta}_x \zeta_\beta(\dot{z})] d\Gamma \\ & + \omega_N \int_{\Gamma_X^c} g^2[(n \cdot e_x(\dot{z}))m_{\alpha\beta}^{-1}(n \cdot \bar{e}_\beta)] d\Gamma \end{aligned} \quad (29)$$

is the same as the linearized contact bilinear form used in Eq. (13) by substituting \dot{z} into Δz , and the contact fictitious load $b'_N(z, \bar{z})$ is defined as

$$b'_N(z, \bar{z}) \equiv b_N^*(z; V, \bar{z}) + \omega_N \int_{\Gamma_X^c} \kappa g \hat{z} \cdot n V_n d\Gamma \quad (30)$$

Since form $b_N^*(z; \bullet, \bullet)$ is computed during response analysis, the same process can be used for DSA with different arguments.

The shape design sensitivity equation is obtained by taking the material derivative of Eq. (9) and by using the relation in Eqs. (17), (18), and (28) as

$$a_\Omega^*(z; \dot{z}, \bar{z}) + b_N^*(z; \dot{z}, \bar{z}) = \ell'_V(\bar{z}) - a'_V(z, \bar{z}) - b'_N(z, \bar{z}) \quad \forall \bar{z} \in Z \quad (31)$$

Note that design sensitivity equation (31) is linear and symmetric with respect to its arguments, and is solved per each design parameter at a given load step. Each design parameter has a different design velocity field V . The same system of equations is solved with different right sides. Since the left side of Eq. (31) is the same as that of Eq. (14) in response analysis, it is very efficient to solve a linear system of equations using an already factorized matrix. In case of elastic material, the fictitious load on the right side of Eq. (31) depends on the design velocity V and on the response analysis result z at the last load step. Thus, the design sensitivity equation is solved only at the last converged load step to obtain \dot{z} and very significant efficiency can be expected in the amount of computational time as compared to incremental nonlinear response analysis. For the elastoplastic problem, however, such efficiency cannot be expected since the structural fictitious load is path dependent.

4. Frictional contact design sensitivity analysis

When friction exists on the contact surface, the structure experiences a tangential traction force, in addition to the normal contact force in Eq. (8). Since the frictional behavior is complicated, many idealizations have been made. The Coulomb friction law is one of the frequently used methods to describe frictional behavior. However, this method presents numerical difficulties because of a discontinuity in the frictional force. A more advanced friction theory assumes that the frictional force elastically increases until it reaches the limit value, and then the macroscopic slip occurs along the contact surface. This theory corresponds to the nonassociative flow rule in elastoplasticity. Thus, a similar return-mapping algorithm can be used to determine the frictional force. In this section, a design sensitivity formulation of this frictional model is developed.

4.1. Friction model

The frictional force appears parallel to the contact surface and is expressed as

$$\mathbf{f} = f_x \mathbf{e}^x \tag{32}$$

The friction form of the contact problem can then be defined by multiplying the frictional force by the virtual relative slip (Laursen and Simo, 1993) as

$$b_T(\mathbf{z}, \bar{\mathbf{z}}) = \int_{\Gamma_c} f_x \bar{\xi}_x \, d\Gamma \tag{33}$$

The expression of $\bar{\xi}_x$ can be obtained by taking the variation of consistency condition in Eq. (3) as

$$A_{\alpha\beta} \bar{\xi}_x = \hat{\mathbf{z}} \cdot \mathbf{e}_\beta - \mathbf{g}\mathbf{n} \cdot \bar{\mathbf{z}}_{,\beta} \tag{34}$$

From its definition in Eq. (27), the coefficient matrix $A_{\alpha\beta}$ contains the second-order derivative of the contact surface. Thus, the contact surface has to be C^2 -continuous in order to have a continuous friction force. The regularity requirement of the contact surface will be discussed in detail in Section 5.

In the regularized frictional model, frictional force f_x is calculated by using a return-mapping algorithm like in elastoplasticity, as shown in Fig. 4. In Fig. 4, the right superscript “tr” denotes the elastic trial status, and “ $n - 1$ ” denotes the previous configuration time t_{n-1} . In addition, $M_{\alpha\beta} = \mathbf{E}_\alpha \cdot \mathbf{E}_\beta$ and \mathbf{E}_α is the tangential vector at the undeformed configuration. Initially, the frictional force increases in proportion to the relative slip amount. This trial frictional force is then compared with the limit value $\mu\omega_N g$. If the trial force is smaller than the limit value, then the trial force becomes the frictional force (stick condition). If the trial force is greater than the limit value, then the limit value is used for the frictional force (slip condition). Note that the direction of the frictional force is parallel to the trial force.

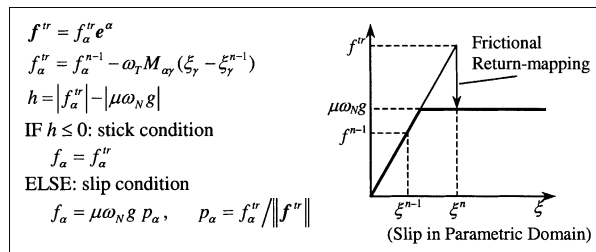


Fig. 4. Return-mapping algorithm for the frictional force.

As with the frictionless contact problem, the nonlinear friction form in Eq. (33) has to be linearized as part of the implicit solution process. The linearized friction form is denoted by $b_T^*(\mathbf{z}; \Delta\mathbf{z}, \bar{\mathbf{z}})$, an expression that is developed in the following section. If the following definitions are made,

$$\begin{aligned} b_T(\mathbf{z}, \bar{\mathbf{z}}) &= b_N(\mathbf{z}, \bar{\mathbf{z}}) + b_T(\mathbf{z}, \bar{\mathbf{z}}) \\ b_T^*(\mathbf{z}; \Delta\mathbf{z}, \bar{\mathbf{z}}) &= b_N^*(\mathbf{z}; \Delta\mathbf{z}, \bar{\mathbf{z}}) + b_T^*(\mathbf{z}; \Delta\mathbf{z}, \bar{\mathbf{z}}) \end{aligned} \quad (35)$$

then linearized incremental equation (14) can be extended to the frictional contact problem as

$$a_\Omega^*(\mathbf{z}^k; \Delta\mathbf{z}^{k+1}, \bar{\mathbf{z}}) + b_T^*(\mathbf{z}^k; \Delta\mathbf{z}^{k+1}, \bar{\mathbf{z}}) = \ell_\Omega(\bar{\mathbf{z}}) - a_\Omega(\mathbf{z}^k, \bar{\mathbf{z}}) - b_T(\mathbf{z}^k, \bar{\mathbf{z}}) \quad \forall \bar{\mathbf{z}} \in Z \quad (36)$$

It is shown in the next section that the same left side of Eq. (36) can be used in DSA.

4.2. Design sensitivity formulation of friction form

Unlike the frictionless contact form in Eq. (8), the friction form depends on analysis results at the previous load step because of the updating algorithm of the frictional force, as explained in Fig. 4. Thus, the sensitivity equation constitutes three parts: implicitly dependent terms, explicitly dependent terms, and path-dependent terms. The material derivative of the friction form can be obtained from Eq. (33) as

$$\frac{d}{d\tau} [b_T(\mathbf{z}, \bar{\mathbf{z}})] \Big|_{\tau=0} = \int_{\Gamma_x^c} (\dot{f}_x \bar{\xi}_x + f_x \dot{\bar{\xi}}_x + \kappa f_x \bar{\xi}_x \dot{V}_n) d\Gamma \quad (37)$$

As explained in Section 3.2, the last term in Eq. (37) can be calculated from analysis results and design velocity information. The expression of $\dot{\bar{\xi}}$ can be obtained by differentiating Eq. (34) with respect to the design parameter as

$$\begin{aligned} A_{\alpha\beta} \dot{\bar{\xi}}_\alpha &= -\mathbf{e}_x \cdot \hat{\mathbf{z}}_{,\beta} \dot{\xi}_\beta - \mathbf{e}_x \cdot (\hat{\mathbf{z}}_{,\beta} + \hat{\mathbf{V}}_{,\beta}) \bar{\xi}_\beta - (\mathbf{e}_x \cdot \mathbf{x}_{,\beta\gamma}^c - \mathbf{g}\mathbf{n} \cdot \mathbf{x}_{,\alpha\beta\gamma}^c) \bar{\xi}_\beta \dot{\xi}_\gamma - \bar{\xi}_\beta \mathbf{e}_\beta \cdot \dot{\mathbf{e}}_x - \dot{\xi}_\beta \mathbf{e}_\beta \cdot \bar{\mathbf{e}}_x \\ &\quad + \mathbf{g}\mathbf{n} \cdot \hat{\mathbf{z}}_{,\alpha\beta} \dot{\xi}_\beta + \mathbf{g}\mathbf{n} \cdot (\hat{\mathbf{z}}_{,\alpha\beta} + \hat{\mathbf{V}}_{,\alpha\beta}) \bar{\xi}_\beta + \hat{\mathbf{z}} \cdot \dot{\mathbf{e}}_x + (\hat{\mathbf{z}} + \hat{\mathbf{V}}) \cdot \bar{\mathbf{e}}_x \end{aligned} \quad (38)$$

Note that Eq. (38) includes the implicitly dependent ($\hat{\mathbf{z}}$) and the explicitly dependent term (\mathbf{V}). No path-dependent term exists, and the expression is the same for both stick and slip conditions. Also, note that the coefficient of the implicit and explicit term is the same, which will be convenient in the sensitivity implementation stage.

With the stick condition, the traction force increases in proportional to the amount of relative slip between two contact surfaces. This increase corresponds to the elastic status of elastoplasticity. The material derivative of the frictional force contains three contributions as

$$\begin{aligned} \dot{f}_x &= \omega_T \Phi_{\alpha\beta} \dot{\xi}_\beta(\hat{\mathbf{z}}) && : \text{implicit} \\ &+ \omega_T \Phi_{\alpha\beta} \dot{\xi}_\beta(\mathbf{V}) && : \text{explicit} \\ &+ \dot{f}_x^{n-1} + \omega_T M_{\alpha\beta} \xi_\beta^{n-1}(\hat{\mathbf{z}}) && : \text{path-dependent} \end{aligned} \quad (39)$$

where $\Phi_{\alpha\beta} = M_{\alpha\beta} + M_{\alpha\gamma,\beta} (\dot{\xi}_\gamma - \xi_\gamma^{n-1})$. Thus, the material derivative of the frictional force depends on sensitivity results at the previous load step, which makes the sensitivity equation path dependent. Again, note that the expressions of implicit and explicit terms are the same if $\hat{\mathbf{z}}$ is replaced by \mathbf{V} .

By substituting Eqs. (38) and (39) into Eq. (37), the material derivative of the friction form is explicitly obtained in terms of, $\dot{\mathbf{z}}$, \mathbf{V} , and the path-dependent terms, as

$$\frac{d}{d\tau} [b_T(\mathbf{z}, \bar{\mathbf{z}})] \Big|_{\tau=0} \equiv b_T^*(\mathbf{z}; \dot{\mathbf{z}}, \bar{\mathbf{z}}) + b_T'(\mathbf{z}, \bar{\mathbf{z}}) \quad (40)$$

where the linearized friction form is defined by collecting all terms that include $\dot{\mathbf{z}}$ as

$$b_T^*(\mathbf{z}; \dot{\mathbf{z}}, \bar{\mathbf{z}}) = \int_{\Gamma_X^c} \left\{ \omega_T \Phi_{\alpha\beta} \bar{\xi}_\alpha \bar{\xi}_\beta(\dot{\mathbf{z}}) + f_\gamma A_{xy}^{-1} [-\mathbf{e}_\alpha \cdot \hat{\mathbf{z}}_{,\beta} \bar{\xi}_\beta(\dot{\mathbf{z}}) - \mathbf{e}_\alpha \cdot \hat{\mathbf{z}}_{,\beta} \bar{\xi}_\beta - (\mathbf{e}_\alpha \cdot \mathbf{x}_{,\beta\zeta}^c - \mathbf{g}\mathbf{n} \cdot \mathbf{x}_{,\alpha\beta\zeta}^c) \bar{\xi}_\beta \bar{\xi}_\zeta(\dot{\mathbf{z}}) - \bar{\xi}_\beta \mathbf{e}_\beta \cdot \mathbf{e}_\alpha(\dot{\mathbf{z}}) - \bar{\xi}_\beta(\dot{\mathbf{z}}) \mathbf{e}_\beta \cdot \bar{\mathbf{e}}_\alpha + \mathbf{g}\mathbf{n} \cdot \hat{\mathbf{z}}_{,\alpha\beta} \bar{\xi}_\beta(\dot{\mathbf{z}}) + \mathbf{g}\mathbf{n} \cdot \hat{\mathbf{z}}_{,\alpha\beta} \bar{\xi}_\beta + m_{\beta\zeta}^{-1} (\hat{\mathbf{z}} \cdot \mathbf{e}_\beta \mathbf{e}_\zeta \cdot \hat{\mathbf{z}}_{,\alpha} + \hat{\mathbf{z}} \cdot \mathbf{e}_\beta \mathbf{e}_\zeta \cdot \hat{\mathbf{z}}_{,\alpha}) + \hat{\mathbf{z}} \cdot \mathbf{nn} \cdot \mathbf{e}_\alpha(\dot{\mathbf{z}}) + \bar{\mathbf{e}}_\alpha \cdot \mathbf{nn} \cdot \hat{\mathbf{z}}] \right\} d\Gamma \quad (41)$$

and the friction fictitious load is obtained by collecting those explicitly dependent terms and path-dependent terms as

$$b_T'(\mathbf{z}, \bar{\mathbf{z}}) = b_T^*(\mathbf{z}; \mathbf{V}, \bar{\mathbf{z}}) + \int_{\Gamma_X^c} \kappa f_\alpha \bar{\xi}_\alpha V_n d\Gamma + \int_{\Gamma_X^c} (\dot{f}_\alpha^{n-1} \bar{\xi}_\alpha + \omega_T M_{\alpha\beta} \bar{\xi}_\alpha \dot{\xi}_\beta^{n-1}) d\Gamma \quad (42)$$

Note that the last integral represents those path-dependent terms that are obtained from the design sensitivity results at the previous load step t_{n-1} .

With the slip condition, the magnitude of the frictional force is determined from the normal contact force, while the applied direction is still parallel to the trial force. From the return-mapping algorithm in Fig. 4, the material derivative of the frictional force for the slip condition can be obtained as

$$\dot{f}_\alpha = \mu \omega_N p_\alpha \mathbf{n} \cdot (\hat{\mathbf{z}} + \hat{\mathbf{V}}) + \frac{\mu \omega_N \mathbf{g}}{\|\mathbf{f}^{\text{tr}}\|} [\dot{f}_\alpha^{\text{tr}} - p_\alpha p^\beta \dot{f}_\beta^{\text{tr}} - f_\alpha^{\text{tr}} p_\alpha \mathbf{P} \cdot \dot{\mathbf{e}}^\beta] \quad (43)$$

where $\dot{f}_\alpha^{\text{tr}}$ is exactly the same as in Eq. (39) for the stick condition. By substituting Eqs. (38) and (43) into Eq. (37), the material derivative of the friction form is obtained. If the implicitly dependent terms are combined, then the following linearized friction form is defined:

$$b_T^*(\mathbf{z}; \dot{\mathbf{z}}, \bar{\mathbf{z}}) = \mu \omega_N \int_{\Gamma_X^c} \left[\mathbf{n} \cdot \hat{\mathbf{z}} p_\alpha \bar{\xi}_\alpha - \omega_T \mathbf{g} (\delta_\alpha^\beta - p_\alpha p^\beta) \Phi_{\beta\gamma} \bar{\xi}_\alpha \bar{\xi}_\gamma(\dot{\mathbf{z}}) / \|\mathbf{f}^{\text{tr}}\| \right] d\Gamma + \mu \omega_N \int_{\Gamma_X^c} \left[g p_\alpha p^\beta \bar{\xi}_\alpha (\hat{\mathbf{z}}_{,\alpha} \cdot \mathbf{p} - \mathbf{x}_{,\alpha\beta}^c \cdot \mathbf{p} \bar{\xi}_\beta(\dot{\mathbf{z}})) d\Gamma + \int_{\Gamma_X^c} f_\gamma A_{xy}^{-1} [-\mathbf{e}_\alpha \cdot \hat{\mathbf{z}}_{,\beta} \bar{\xi}_\beta(\dot{\mathbf{z}}) - \mathbf{e}_\alpha \cdot \hat{\mathbf{z}}_{,\beta} \bar{\xi}_\beta - (\mathbf{e}_\alpha \cdot \mathbf{x}_{,\beta\zeta}^c - \mathbf{g}\mathbf{n} \cdot \mathbf{x}_{,\alpha\beta\zeta}^c) \bar{\xi}_\beta \bar{\xi}_\zeta(\dot{\mathbf{z}}) - \bar{\xi}_\beta \mathbf{e}_\beta \cdot \mathbf{e}_\alpha(\dot{\mathbf{z}}) - \bar{\xi}_\beta(\dot{\mathbf{z}}) \mathbf{e}_\beta \cdot \bar{\mathbf{e}}_\alpha + \mathbf{g}\mathbf{n} \cdot \hat{\mathbf{z}}_{,\alpha\beta} \bar{\xi}_\beta(\dot{\mathbf{z}}) + \mathbf{g}\mathbf{n} \cdot \hat{\mathbf{z}}_{,\alpha\beta} \bar{\xi}_\beta + m_{\beta\zeta}^{-1} (\hat{\mathbf{z}} \cdot \mathbf{e}_\beta \mathbf{e}_\zeta \cdot \hat{\mathbf{z}}_{,\alpha} + \hat{\mathbf{z}} \cdot \mathbf{e}_\beta \mathbf{e}_\zeta \cdot \hat{\mathbf{z}}_{,\alpha}) + \hat{\mathbf{z}} \cdot \mathbf{nn} \cdot \mathbf{e}_\alpha(\dot{\mathbf{z}}) + \bar{\mathbf{e}}_\alpha \cdot \mathbf{nn} \cdot \hat{\mathbf{z}}] d\Gamma \right] \quad (44)$$

In a similar way, the explicitly dependent terms and path-dependent terms are combined to define the friction fictitious load as

$$b_T'(\mathbf{z}, \bar{\mathbf{z}}) = b_T^*(\mathbf{z}; \mathbf{V}, \bar{\mathbf{z}}) + \int_{\Gamma_X^c} \kappa f_\alpha \bar{\xi}_\alpha V_n d\Gamma + \mu \omega_N \int_{\Gamma_X^c} \frac{\mathbf{g} \bar{\xi}_\beta}{\|\mathbf{f}^{\text{tr}}\|} (\delta_\alpha^\beta - p_\alpha p^\beta) (\dot{f}_\alpha^{n-1} + \omega_T M_{\alpha\gamma} \dot{\xi}_\gamma^{n-1}) d\Gamma \quad (45)$$

The last integral in Eq. (45) represents the path-dependent terms. It is interesting to note that the form $b_T^*(\mathbf{z}; \dot{\mathbf{z}}, \bar{\mathbf{z}})$ from the stick condition in Eq. (41) is symmetric with respect to its arguments, while $b_T^*(\mathbf{z}; \dot{\mathbf{z}}, \bar{\mathbf{z}})$ from the slip condition in Eq. (44) is not symmetric. This is due to the nonassociative plastic return-mapping algorithm.

By adding Eqs. (30) and (42) for the stick condition, or Eqs. (30) and (45) for the slip condition, the following form can be defined:

$$b_V'(\mathbf{z}, \bar{\mathbf{z}}) = b_V'(\mathbf{z}, \bar{\mathbf{z}}) + b_T'(\mathbf{z}, \bar{\mathbf{z}}) \quad (46)$$

Eq. (46) represents the explicitly dependent and the path-dependent terms of the contact condition. As mentioned before, since the explicitly dependent terms have the same form as the implicitly dependent ones, $b_V'(\mathbf{z}, \bar{\mathbf{z}})$ uses the same contact stiffness matrix from contact analysis. Only path-dependent terms need to be calculated separately.

By adding the material derivative of the friction form in Eq. (40) to Eq. (31), the design sensitivity equation for the frictional contact problem is obtained as

$$a_{\Omega}^*(\mathbf{z}; \dot{\mathbf{z}}, \bar{\mathbf{z}}) + b_r^*(\mathbf{z}; \dot{\mathbf{z}}, \bar{\mathbf{z}}) = \ell'_V(\bar{\mathbf{z}}) - a'_V(\mathbf{z}, \bar{\mathbf{z}}) - b'_V(\mathbf{z}, \bar{\mathbf{z}}) \quad \forall \bar{\mathbf{z}} \in Z \tag{47}$$

This design sensitivity equation solves for the material derivative $\dot{\mathbf{z}}$ for each design variable. Since the left side of Eq. (47) is same as the left side of Eq. (36), the design sensitivity equation uses the same stiffness matrix as response analysis that already has a factorized form. After solving for $\dot{\mathbf{z}}$ at load step t_n , the path-dependent terms have to be updated for the next time step. Since path dependency comes from the frictional force update, the material derivative \dot{f}_x in Eq. (39) or in (43) has to be stored. It is unnecessary to store the material derivative $\dot{\xi}_z$, because Eq. (26) can be used from the calculated $\dot{\mathbf{z}}$. In addition to the frictional effect, the plastic variables of elastoplasticity are path dependent, and their material derivatives have to be updated accordingly (see Kim et al. (2001)).

5. Smooth contact surface

In the development of continuum-based contact analysis and design sensitivity formulation, it can easily be seen that the expression of the contact force in Eq. (33) contains the second-order derivative of the master surface, while the linearized contact form in Eqs. (41) and (44) contains the third-order derivative of the master surface. Thus, in order to have a continuous contact force as well as a stable Newton method, the master surface should have at least C^2 -continuity. If a conventional finite element-based contact surface representation method is used, discontinuity may occur because it is difficult to impose a C^2 -continuity across the element boundary. One remedy for this difficulty is to generate a C^2 -continuous spline surface using finite element nodes as control points (Hanssen and Klarbring, 1990). However, this approach requires an $n \times m$ regular array of nodes and meshes in order to apply to the 3-D contact surface. Wang (2000) proposed a method to generate a smooth surface from a scattered set of particles without requiring mesh connectivity.

In this paper, a smooth master surface is generated by using a meshfree interpolation function. Since the design sensitivity equation (47) is developed based on the continuum geometry, the same formulation can apply for either a piecewise linear surface or a smooth surface without any modification. The sensitivity formulation only requires information that is already available from contact analysis. However, if a discrete design sensitivity formulation is used, then the differentiation of the surface generation process has to be taken into account, which is not only complicated but strongly depends on the analysis code.

Fig. 5 shows the process of constructing a smooth surface from a set of scattered particles using a meshfree shape function $\Psi(\xi_1, \xi_2)$. At a given slave particle \mathbf{x} , an NP number of master particles close to the slave particle is selected to construct a local surface. These master particles are then projected onto a parametric plane by using the least-squares method. In the parametric plane, a meshfree interpolation is carried out using those projected particles. Let (ξ_1^I, ξ_2^I) , $I = 1, \dots, \text{NP}$, be the parametric coordinates of the projected particles. The meshfree shape function can be obtained by imposing the reproducing condition as

$$\Psi_I(\xi_1, \xi_2) = \mathbf{H}^T(0, 0) \mathbf{M}^{-1}(\xi_1, \xi_2) \mathbf{H}(\xi_1 - \xi_1^I, \xi_2 - \xi_2^I) \Phi_a(\xi_1 - \xi_1^I, \xi_2 - \xi_2^I) \tag{48}$$

where $\mathbf{H}(\xi_1, \xi_2)$ is the monomial basis vector and is determined by the order of consistency condition. In case of the second-order consistency condition, it becomes

$$\mathbf{H}(\xi_1, \xi_2) = [1 \quad \xi_1 \quad \xi_2 \quad \xi_1^2 \quad \xi_1 \xi_2 \quad \xi_2^2]^T \tag{49}$$

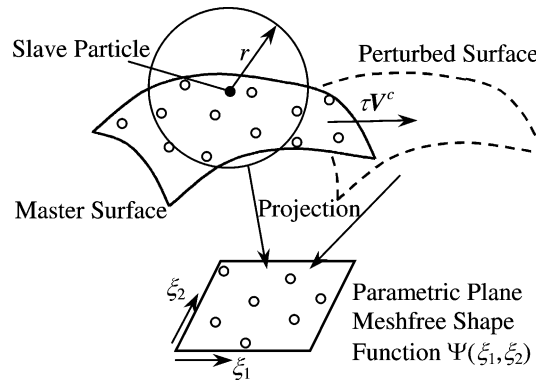


Fig. 5. Construction of a smooth surface from a set of scattered particles.

The moment matrix $\mathbf{M}(\xi_1, \xi_2)$ in Eq. (48) is defined as

$$\mathbf{M}(\xi_1, \xi_2) = \sum_{I=1}^{\text{NP}} \mathbf{H}(\xi_1 - \xi_1^I, \xi_2 - \xi_2^I) \mathbf{H}^T(\xi_1 - \xi_1^I, \xi_2 - \xi_2^I) \Phi_a(\xi_1 - \xi_1^I, \xi_2 - \xi_2^I) \quad (50)$$

Since matrix inversion is involved in Eq. (48), it is important to note that NP has to be large enough so that the matrix \mathbf{M}^{-1} is not singular. Finally, the kernel function $\Phi_a(\xi_1, \xi_2)$ determines the smoothness of the shape function $\Psi(\xi_1, \xi_2)$. Since a minimum of C^2 -continuity is required for the master surface, the kernel function can be selected from the C^2 cubic B-spline function or from the C^∞ Gaussian function.

After generating the meshfree shape function in the parametric domain, the physical coordinate and the tangential vectors of the master surface can be interpolated using

$$\mathbf{x}(\xi_1, \xi_2) = \sum_{I=1}^{\text{NP}} \Psi_I(\xi_1, \xi_2) \mathbf{x}_I \quad (51)$$

$$\mathbf{x}_{,\alpha}(\xi_1, \xi_2) = \sum_{I=1}^{\text{NP}} \frac{d\Psi_I(\xi_1, \xi_2)}{d\xi_\alpha} \mathbf{x}_I \quad (52)$$

Thus, all geometric variables that appear in previous chapters can be calculated.

6. Numerical examples

In order to show the applicability of the proposed contact analysis and DSA methods, 2-D and 3-D numerical examples are provided.

6.1. Design optimization of a rubber gasket

An engine gasket is used to prevent oil leakage. The purpose of the design is to determine the shape of the gasket so that open areas are minimized after installation. Although open areas can be minimized by increasing the gasket size or by applying a large amount of installation force, such methods can cause stress concentration, and thus, a short service life.

Fig. 6 shows the initial gasket geometry before installation. Since the engine block is much stiffer than the rubber gasket, only the gasket is modeled, using a meshfree method with 325 particles; it is assumed that all other parts are rigid. A Mooney–Rivlin hyperelastic material (Chen et al., 1998) is used with

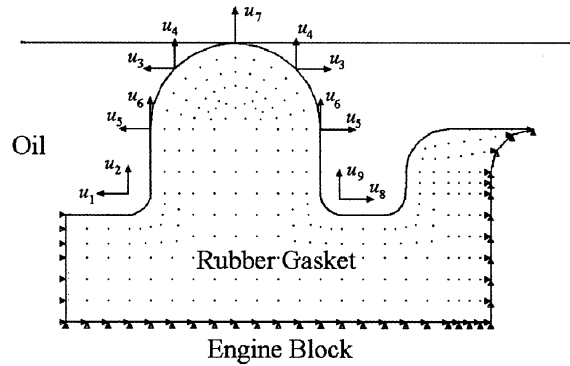


Fig. 6. Design parameterization of the gasket.

$C_{01} = 80 \text{ kPa}$, $C_{10} = 20 \text{ kPa}$, and bulk modulus $k = 10^4$. A constant frictional coefficient $\mu = 0.05$ is used for all contact interfaces. Parametric spline curves are used to represent the gasket boundary, and the shapes of these curves are defined as design parameters. Nine shape design parameters are defined, as shown in Fig. 6. In order to maintain the symmetrical shape, four design parameters are linked. A Newton iterative method is used to solve the nonlinear structural equation with 100 load steps. If the incremental time step size is determined based on deformation, then the variation of the time step size affects the sensitivity result, which is important in the explicit time integration method. Since the implicit method is used in this paper, the time step size is fixed and the effect of time step size does not appear in the sensitivity expression. DSA is carried out at each converged load step to solve the displacement sensitivity. After it is solved, the sensitivities of various performance measures are calculated using the chain rule of differentiation. Fig. 7 shows the deformed geometry and the hydrostatic pressure plot of the gasket after installation. As the gasket deforms, a self-contact occurs in the corner region, where a severe material distortion is observed. As can be seen in Fig. 7, the open area after installation is denoted by d , which will be minimized during the design optimization process.

Design optimization of the engine gasket-sealing problem is solved to minimize the open gap after installation. Since the performance of the gasket is determined by the contact force (F_C) and the contact region between interfaces, design constraints are applied to maintain a minimum of contact force and contact area. Since the contact region cannot be defined before analysis, a possible contact region is initially

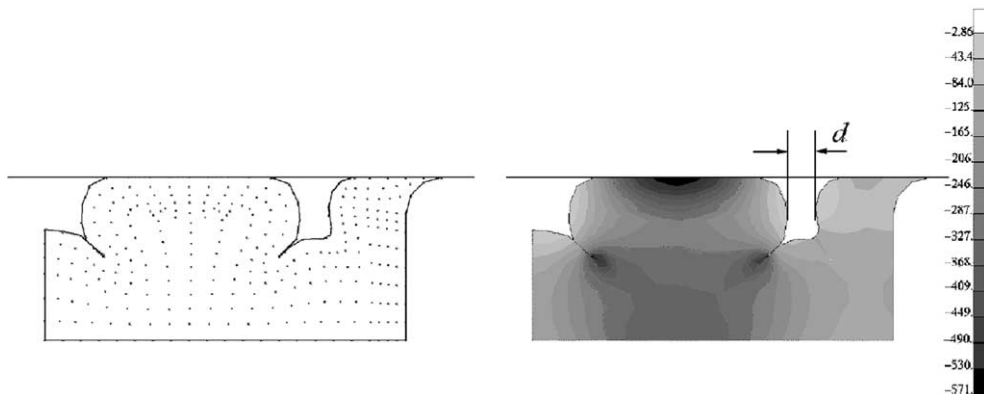


Fig. 7. Meshfree analysis result at the initial design.

defined, and the square sum of the gap ($\sum \text{gap}^2$) along the region is then measured as a constraint. In addition, the maximum value of the von Mises stress (σ_{VM}) is considered as a constraint. The design optimization problem is defined by

$$\begin{aligned}
 &\text{minimize} && d \\
 &\text{subject to} && |F_C| \geq 300 \text{ kN} \\
 &&& \sum \text{gap}^2 \leq 1.0 \text{ mm} \\
 &&& \sigma_{\text{VM}} \leq 1700 \text{ kPa} \\
 &&& -0.5 \leq u_i \leq 0.5
 \end{aligned} \tag{53}$$

where the objective function d is the open gap as shown in Fig. 7, and u_i , $i = 1, \dots, 9$, is the shape design parameters as shown in Fig. 6.

The analysis results from the initial design are used to determine the reference values of constraints. The design optimization problem in Eq. (53) is solved using a sequential quadratic programming method in design optimization tool (Vanderplaats, 1997), and the optimization problem is converged after 13 iterations. Fig. 8 shows the optimum geometry and pressure plots. The open gap in the initial design is significantly reduced at the optimum design. It is interesting to note that the initial circular region of the gasket top changes to an H-shape at the optimum design in order to reduce the concentration of stress, while increasing the contact region. Fig. 9 shows the history of the cost function. A majority of the open gap is reduced within four iterations, and the remainder is used to improve constraint violations. Such fast convergence of the optimization algorithm can be explained by the accurate design sensitivity information.

6.2. Design sensitivity analysis of a metal punch problem

2-D DSA is further extended to a 3-D elastoplastic contact problem, as shown in Fig. 10. In this problem, the plate thickness and radius of a circular rigid surface are chosen as design parameters. A total of 558 particles are used in the discretization of the plate, and a total of 308 particles are used to represent rigid surfaces. The plate is assumed to be an elastoplastic material with the following material properties: $E = 207 \text{ GPa}$, $\nu = 0.29$, $\sigma_Y = 167 \text{ MPa}$, $H = 772 \text{ MPa}$. A nonlinear meshfree analysis is carried out with 50 load steps, accompanied by DSA. As illustrated in Fig. 11, the whole structure is within the plastic range. The computational cost of DSA per design parameter is about 8.3% of the response analysis cost, which is very efficient compared to the finite difference method. The vertical displacement sensitivity results are

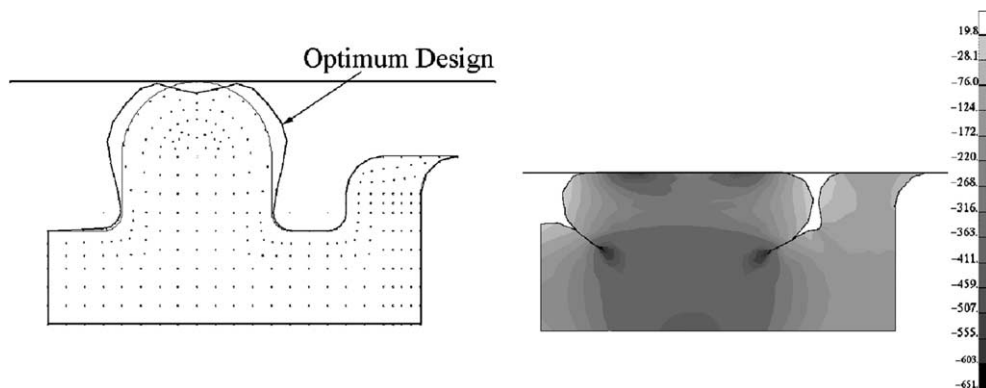


Fig. 8. Meshfree analysis result at the optimum design.

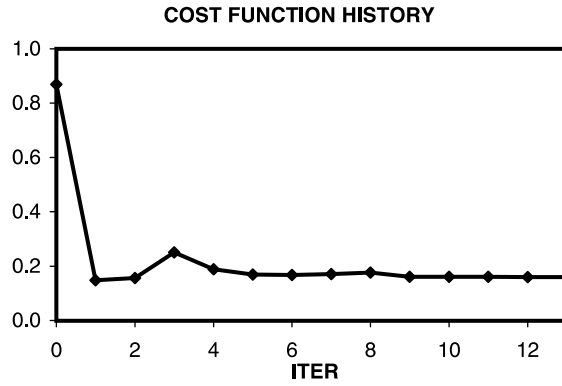


Fig. 9. Cost function history of the gasket problem.

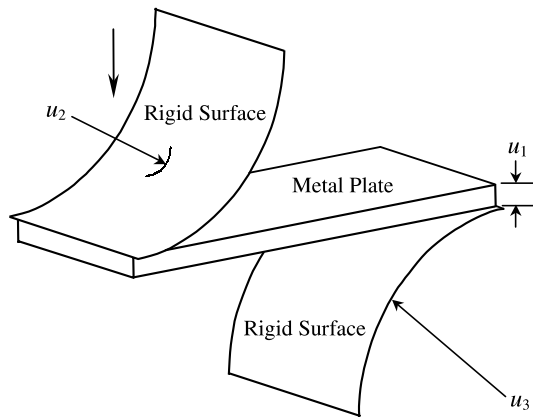


Fig. 10. Analysis model of metal punch problem.

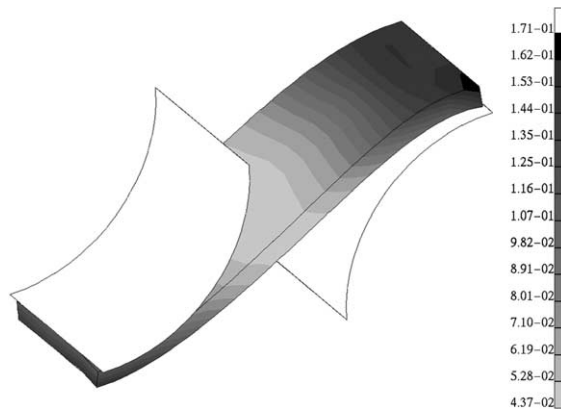


Fig. 11. Deformed shape and plastic strain plot of the punch problem.

Table 1
Accuracy of design sensitivity results

Design	Performance	ψ	$\Delta\psi$	$\psi' \Delta\tau$	$\Delta\psi/\psi' \Delta\tau \times 100$
u_1	Z344	-7.66403	-8.74269E-7	-8.74284E-7	100.00
	Z331	-7.11372	-8.70281E-7	-8.70297E-7	100.00
	Z319	-6.46946	-8.41994E-7	-8.42008E-7	100.00
	Z307	-5.78084	-7.79330E-7	-7.79347E-7	100.00
	Z295	-5.07427	-6.83249E-7	-6.83270E-7	100.00
	Z283	-4.36168	-5.64229E-7	-5.64249E-7	100.00
	Z271	-3.64779	-4.38470E-7	-4.38491E-7	100.00
	Z259	-2.93541	-3.23620E-7	-3.23641E-7	99.99
	Z286	-4.33574	-5.13241E-7	-5.13267E-7	100.00
	Z312	-5.77780	-7.17279E-7	-7.17305E-7	100.00
u_2	Z344	-7.66403	1.01763E-6	1.01722E-6	100.04
	Z331	-7.11372	9.93909E-7	9.93374E-7	100.05
	Z319	-6.46946	9.34760E-7	9.34128E-7	100.07
	Z307	-5.78084	8.48858E-7	8.48161E-7	100.08
	Z295	-5.07427	7.46921E-7	7.46197E-7	100.10
	Z283	-4.36168	6.36105E-7	6.35389E-7	100.11
	Z271	-3.64779	5.21189E-7	5.20510E-7	100.13
	Z259	-2.93541	4.05932E-7	4.05317E-7	100.15
	Z286	-4.33574	6.24759E-7	6.23955E-7	100.13
	Z312	-5.77780	8.39500E-7	8.38630E-7	100.10
u_3	Z344	-7.66403	-1.73855E-7	-1.73653E-7	100.12
	Z331	-7.11372	-3.13213E-7	-3.12915E-7	100.10
	Z319	-6.46946	-5.02555E-7	-5.02153E-7	100.08
	Z307	-5.78084	-7.15329E-7	-7.14828E-7	100.07
	Z295	-5.07427	-9.30001E-7	-9.29415E-7	100.06
	Z283	-4.36168	-1.13062E-6	-1.12997E-6	100.06
	Z271	-3.64779	-1.30268E-6	-1.30198E-6	100.05
	Z259	-2.93541	-1.43077E-6	-1.43006E-6	100.05
	Z286	-4.33574	-1.46946E-6	-1.46873E-6	100.05
	Z312	-5.77780	-1.28150E-6	-1.28086E-6	100.05

compared with the finite difference results in Table 1, with excellent agreements. In Table 1, column ψ is the value of the performance measure (vertical displacement), column $\Delta\psi$ is the finite difference result with the perturbation size $\Delta\tau = 10^{-6}$, $\psi' \Delta\tau$ is the first-order approximation using the proposed sensitivity results, and the last column is the ratio between the finite difference and the proposed method.

6.3. Design of an extrusion problem

A design optimization of the extrusion problem is considered in order to improve the product quality and to reduce the processing cost. Product quality is related to the final product shape and the regularity of the product's mechanical properties. The processing cost is related to the process control force, deformation work, or deformation efficiency. In addition, process limits have to be considered in the design stage, such as the maximum contact stress level that will result in die failure and punch buckling.

In this example, a forward solid extrusion problem, as illustrated in Fig. 12, is considered. In displacement-driven nonlinear analysis, the vertical displacement of the billet's upper surface is controlled to push it down. Then, the reaction force on the billet's top surface is measured as the process control force. Because of the symmetry, a quarter model is used with the symmetric boundary conditions. The ratio of the area reduction is 2.65, and the initial die angle is 30° . The whole die surface is modeled with a 612 number

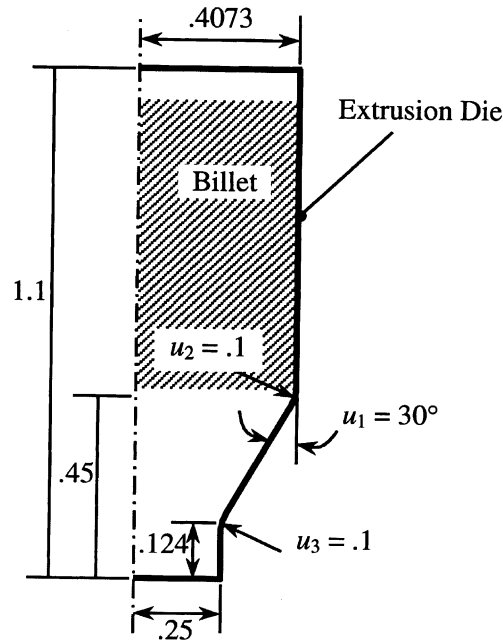


Fig. 12. Design parameters for the circular–circular extrusion problem.

of particles, and a smooth contact surface is locally generated based on the meshfree approximation method in Eq. (51). A contact constraint is imposed between the billet's outer surface and the extrusion die surface with the frictional coefficient of $\mu = 0.05$.

Fig. 13 shows the deformation history and the effective plastic strain at the final configuration. The maximum effective plastic strain appears at the outer surface of the billet with the magnitude of 2.68. The initial billet length of 0.6 m is extended to 1.6583 m at the final configuration, which corresponds to 276% extension. This extension ratio conforms to the area reduction ratio 2.65 and the maximum plastic strain 2.68.

Since the extrusion process generates the desired final shape from a circular billet, design parameters are mostly limited to the extrusion die shape and the material property. The material property design parameter can be considered since it is possible to adjust the material property by changing the process temperature. In addition, the frictional coefficient can be considered as a design parameter. In this example, the die shape represents the die depth, the die angle, and dead zone fillet radius. As illustrated in Fig. 12, three design parameters are defined on the circular die. As explained in Section 3, the design velocity field that corresponds to the design parameter must be defined on the extrusion die surface. Fig. 14 shows the vector plots of three design parameters. As design changes, particle points on the die surface will move in the direction of the design velocity vector.

DSA is carried out using the design velocity fields defined in Fig. 14. The process work and the maximum plastic strain are chosen as performance measures. The computational cost of DSA is about 10% of the response analysis cost per design parameter. Table 2 shows the design sensitivity of the process force and the maximum effective plastic strain. The design parameter u_1 contributes to the process force the most significantly, while the design parameters u_2 and u_3 contribute to the effective plastic strain.

Since the design parameter u_1 (the die angle) contributes the most to the process work, a new updated design is generated by reducing the die angle to 27° , which is a 10% reduction from the initial design. Fig. 15

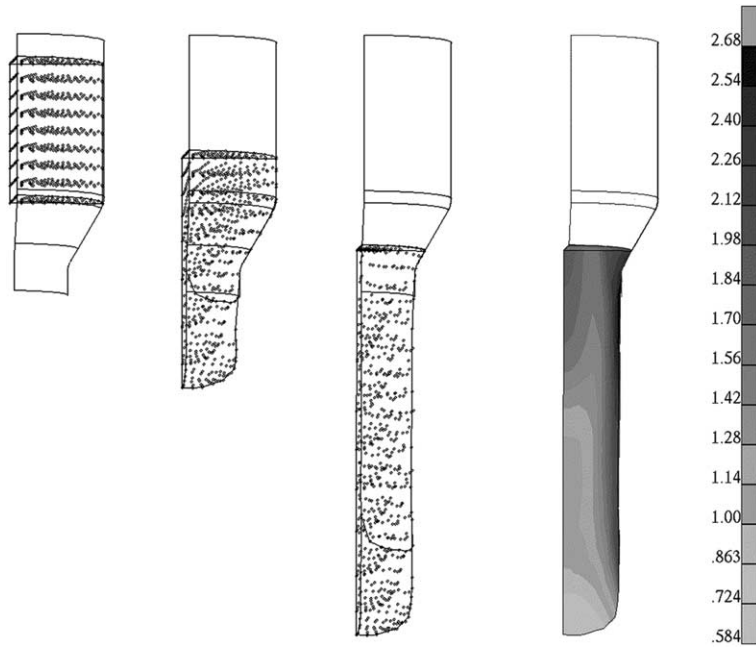


Fig. 13. Deformation history and effective plastic strain of the extrusion problem.

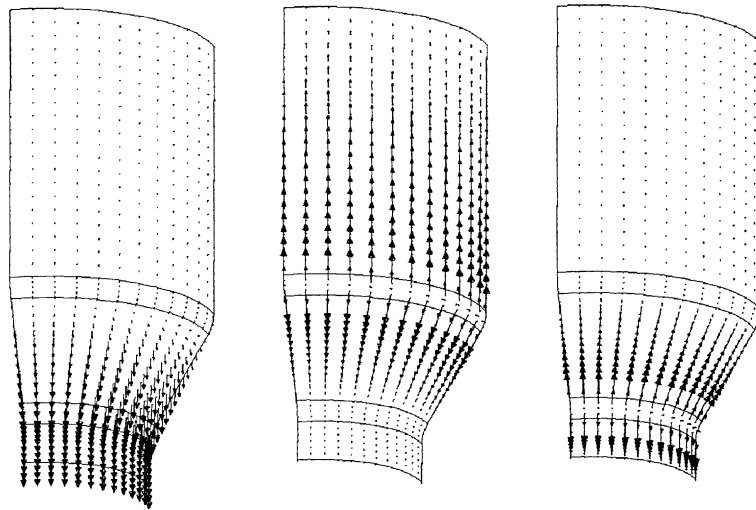


Fig. 14. Design velocity fields: (a) u_1 , (b) u_2 , (c) u_3 .

Table 2
Relative design sensitivity results for the extrusion problem

Design parameter	Process work sensitivity	Plastic strain sensitivity
u_1	$-5.50E-3$	$-5.32E-2$
u_2	$6.60E-4$	$-6.24E-3$
u_3	$-6.65E-5$	$-1.10E-4$

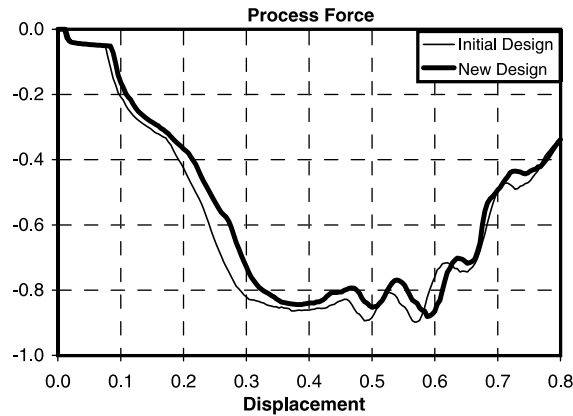


Fig. 15. Extrusion process forces at the initial and new designs.

shows the normalized extrusion process forces at the initial and new designs. The area covered by the process force is the process work. As expected from the design sensitivity results, the process work is reduced by 4.5% for the new design.

7. Conclusion

A DSA and optimization procedure for the contact problem is proposed using the material derivative approach. Since the explicitly dependent terms have the same expression that appears in the linearization process, the matrix information from contact analysis is readily used for the design sensitivity purposes. However, the path-dependent terms must be derived separately when the friction exists between contact interfaces. Since the continuum-based formulation is used, the differentiation of the complicated smooth surface construction process was unnecessary, and virtually any surface construction method is applicable without modification of the formulation. The accuracy and efficiency of sensitivity information is compared with finite difference results with excellent agreement.

Acknowledgements

This research is supported by NSF/DARPA Optimized Portable Algorithms of Applications Libraries (OPAAL). This support is gratefully acknowledged.

References

- Antunez, H.J., Kleiber, M., 1996. Sensitivity analysis of metal forming process involving frictional contact in steady state. *Materials Processing Technology*, Vol. 60, No. (1–4), p. 485–491.
- Barthold, F.J., Bischoff, D., 1988. Generalization of Newton type methods to contact problems with friction. *Journal de Mecanique Theorique et Appliquee*, Vol. 7, 97–110 (Suppl. 1) (Special Issue: Numerical Methods in Mechanics of Contact Involving Friction).
- Chen, J.S., Pan, C., Wu, C.T., Liu, W.K., 1996. Reproducing kernel particle methods for large deformation analysis of nonlinear structures. *Computer Methods in Applied Mechanics and Engineering* 139, 195–227.
- Chen, J.S., Wu, C.T., Pan, C., 1998. A pressure projection method for nearly incompressible rubber hyper-elasticity. Part I: theory and Part II: application. *ASME Journal of Applied Mechanics* 63, 862–876.

- Choi, K.K., 1993. Design sensitivity analysis of nonlinear structures. II. Structural optimization: status and premises. *AIAA Progress in Astronautics and Aeronautics* 150, 407–446 (Chapter 16).
- Chung, S.H., Hwang, S.M., 1998. Optimal process design in non-isothermal, non-steady metal forming by the finite element method. *International Journal for Numerical Methods in Engineering* 42, 1343–1390.
- Hanssen, E., Klarbring, A., 1990. Rigid contact modeled by CAD surface. *Engineering Computations* 7, 344–348.
- Hughes, T.J.R., 1987. *The Finite Element Method*. Prentice Hall, Englewood Cliffs, NJ.
- Kikuchi, N., Oden, J.T., 1988. *Contact Problems in Elasticity: A Study of Variational Inequalities and Finite Element Method*. SIAM, Philadelphia, PA.
- Kim, N.H., Choi, K.K., Chen, J.S., Park, Y.H., 2000. Meshless shape design sensitivity analysis and optimization for contact problem with friction. *Computational Mechanics* 25, 157–168.
- Kim, N.H., Choi, K.K., Chen, J.S., 2001. Structural optimization of finite deformation elastoplasticity using continuum-based shape design sensitivity formulation. *Computers and Structures*, Vol. 79, No. 20–21, 1959–1976.
- Klarbring, A., 1986. A mathematical programming approach to three-dimensional contact problems with friction. *Computer Methods in Applied Mechanics and Engineering* 58, 175–200.
- Kwak, B.M., 1991. Complementarity-problem formulation of 3-dimensional frictional contact. *Journal of Applied Mechanics—Transaction of ASME* 58 (1), 134–140.
- Laursen, T.A., Simo, J.C., 1993. A continuum-based finite element formulation for the implicit solution of multibody, large deformation frictional contact problems. *International Journal for Numerical Methods in Engineering* 36, 2451–3485.
- Liu, W.K., Jun, S., Zhang, Y.F., 1995. Reproducing kernel particle methods. *International Journal for Numerical Methods in Fluids* 20, 1081–1106.
- Luenberger, D.G., 1984. *Linear and Nonlinear Programming*. Addison-Wesley, Massachusetts.
- Maniatty, A.M., Chen, M.F., 1996. Shape sensitivity analysis for steady metalforming processes. *International Journal for Numerical Methods in Engineering* 39, 1199–1217.
- Michalowski, R., Mroz, Z., 1978. Associated and non-associated sliding rules in contact friction problems. *Archives of Mechanics* 30, 259–276.
- Mignot, F., 1976. Controle dans les Inequations Variationelles Elliptiques. *Journal of Functional Analysis* 22, 130–185.
- Pollock, G.D., Noor, A.K., 1996. Sensitivity analysis of the contact/impact response of composite structures. *Computers and Structures* 61, 251–269.
- Simo, J.C., 1992. Algorithms for static and dynamic multiplicative plasticity that preserve the classical return mapping schemes of the infinitesimal theory. *Computer Methods in Applied Mechanics and Engineering* 99, 61–112.
- Sokolowski, J., Zolesio, J.P., 1991. *Introduction to Shape Optimization*. Springer-Verlag, Berlin.
- Spivey, C.O., Tortorelli, D.A., 1994. Tangent operators, sensitivity expressions, and optimal design of nonlinear elastica in contact with applications to beams. *International Journal for Numerical Methods in Engineering* 37, 49–73.
- Vanderplaats, G.N., 1997. *DOT User's Manual*. VMA Corp., Colorado Springs, CO.
- Wang, H.P., 2000. Meshfree smooth contact formulation and boundary condition treatments in multi-body contact. Ph.D. thesis, The University of Iowa, Iowa City, IA.
- Zabaras, N., Bao, Y., Srikanth, A., Frazier, W.G., 2000. A continuum lagrangian sensitivity analysis for metal forming process with application to die design problems. *International Journal for Numerical Methods in Engineering* 48, 679–720.
- Zhao, G.Q., Wright, E., Grandhi, R.V., 1997. Preform die shape design in metal forming using an optimization method. *International Journal for Numerical Methods in Engineering* 40, 1213–1230.